

Application of the Fractional Fourier Transform to Image Reconstruction in MRI

Vicente Parot, Carlos Sing–Long, Carlos Lizama, Cristian Tejos *Member, IEEE*, Sergio Uribe, and Pablo Irarrazaval, *Senior Member, IEEE*

Abstract

To obtain good quality images with Magnetic Resonance (MR) it is necessary to have good spatial homogeneity in the B_0 field for the region of imaging. Field homogeneity is difficult to achieve, particularly for short bore magnets and higher fields. When the passive or active shimming are not enough, or when the inhomogeneity comes from differences in susceptibility between adjacent regions within an object, there are several post-processing techniques for correcting the distortions. These techniques do not have a well supported theoretical background with the exception of linear terms. We propose to use the Fractional Fourier Transform (FrFT) for reconstructing the MR signal acquired under the presence of quadratic fields. The FrFT provides a precise theoretical framework for this. In this work we show how the FrFT can be used to understand the distortions and to reconstruct MR data acquired under that condition. We also show examples of reconstruction for simulated and volunteer data under quadratic inhomogeneities obtaining an improved image quality compared with standard Fourier reconstructions. The FrFT opens a new paradigm for understanding and correcting second degree off-resonances with the potential for manufacturing shorter magnets.

Index Terms

Fractional Fourier Transform, Magnetic Resonance Imaging, MRI, Image Reconstruction, Field Inhomogeneities, Off–Resonance Correction.

V. Parot, C. Sing–Long, C. Tejos and P. Irarrazaval are with the Department of Electrical Engineering, Pontificia Universidad Católica de Chile, Vicuña Mackenna 4860, Macul, Santiago, Chile, and with the Biomedical Imaging Center, Pontificia Universidad Católica de Chile, Vicuña Mackenna 4860, Macul, Santiago, Chile.

S. Uribe is with the Department of Radiology, Pontificia Universidad Católica de Chile, Chile, and with the Biomedical Imaging Center, Pontificia Universidad Católica de Chile, Chile.

C. Lizama is with the Department of Mathematics and Computer Science, Universidad de Santiago de Chile, Avenida Libertador Bernardo O’Higgins 3363, Estación Central, Santiago, Chile.

Application of the Fractional Fourier Transform to Image Reconstruction in MRI

I. INTRODUCTION

Magnetic Resonance (MR) imaging and spectroscopy provide a number of practical applications for both clinical and scientific purposes [1], [2]. For this technique it is necessary to have a strong magnetic field with uniform intensity across the entire field of view. However, deviations from the constant magnetic field are inherent to MR systems as uniform fields are physically difficult to achieve and as adjacent regions within the scanned object show different susceptibilities, producing inhomogeneities. Such field variations introduce an accumulating phase over time into the MR signal, which cannot be demodulated easily as it varies spatially. This problem is worse when stronger uniform fields are considered and whenever sequences with long acquisition time are used. High field MR system designs have to observe this limitation, sometimes using secondary coils to correct the field, simply reducing the entire measurement volume or using a local region of interest for each measurement [3], [4]. Passive and active shimming techniques help reducing inhomogeneities and are commonly used, partially correcting first and second order field variations in most cases.

Several image reconstruction methods have been proposed to correct distortions produced by non homogeneous fields, being an active field of research [5], [6], [7], [8], [9], [10], [11], [12], [13]. There is a well known theory background for the linear correction approaches, in which an exact analytical solution is provided [5], [9], but both for second-order and arbitrary field maps there is no such conclusive theory background.

The Fractional Fourier Transform (FrFT) is a generalization of the standard Fourier Transform (FT) by means of the continuous fractional order a , which covers densely the entire transition between image (or time) domain ($a = 0$) and the Fourier domain ($a = 1$) [14]. The FrFT can be defined in several different ways leading to different physical interpretations and thus, it has become useful in many applications [15], [16], [17]. It has been shown that the FT properties are special cases of FrFT properties [14] and further research has been done in discretization [18], [19], fast computation [20], and other aspects of the FrFT related to signal processing [21], [22], [23], [24].

It is of general knowledge that the magnetization of an object under a uniform magnetic field can be related to its FT. Similarly, we noted that the magnetization of an object under a quadratic magnetic field can be related to its FrFT. In fact, the defining integral kernel of the FT presents a correspondence with the MR signal generated by a magnetized object in a uniform magnetic field and thus, it allows reconstructing the object by taking an inverse FT of its MR signal. Equivalently, the kernel that provides the integral definition of the FrFT presents a clear resemblance with the MR signal generated by an object with an underlying quadratic magnetic field, i.e. a field which intensity varies spatially as a second order polynomial. This fact suggested us that there is a framework that allows native MR reconstruction from quadratic fields.

In this manuscript we present a theoretical description of the relationship between the FrFT and the MR signal generated when quadratic magnetic fields are used. Furthermore, we propose a general MR method based on the FrFT that allows the acquisition and reconstruction of MR signals of objects that have been obtained with quadratic fields.

In Section II, we propose a new FrFT-based framework that allows fractional Fourier understanding of the MR signal obtained with quadratic field inhomogeneities, showing examples with simple trajectories. We explain the relationship between the FrFT and the MR signal in a one-dimensional context, which is extended to two dimensions in Section III. We propose a general reconstruction method based on the FrFT in Section IV. In Section V we describe the experimental setup and methods, and in Section VI we show the results of our simulation, phantom and *in-vivo* experiments. Section VII includes further discussions and conclusions from this work and suggestions for future work.

II. THEORY

In this section we explain the relation between the Fractional Fourier Transform and an MR signal acquired under a quadratic main field, showing how the MR signal can be written as a FrFT. This framework allows us to analyze the acquired data in a fractional order polar space, from where we can extract visual insight.

A. Fractional Fourier Transform

The a -th order FrFT $f_a(\rho) = \mathcal{F}^a\{f\}(\rho)$ of the signal $f(u)$ for $0 < |a| < 2$ can be expressed as an integral transform as (taken from [14] with a slight change of notation)

$$f_a(\rho) = C_\alpha(\rho) \int f(u) e^{i\pi(u^2 \cot \alpha - 2\rho u \csc \alpha)} du \quad (1)$$

$$C_\alpha(\rho) \equiv e^{i\pi\rho^2 \cot \alpha} \sqrt{1 - i \cot \alpha}, \quad \alpha \equiv a\pi/2 \quad (2)$$

Note that the most notable difference between this equation and the Fourier transform is an extra quadratic phase in the kernel.

Throughout this section, we have selected u and ρ to denote dimensionless variables in order to maintain formal consistency between the MRI and FrFT contexts. The independent variable ρ is the pseudo-frequency in any fractional domain and u is the particular case of ρ for the 0-th order (the object axis). The relation between the dimensionless u and its dimensional counterpart x will be addressed at the end of Section IV.

B. MRI Signal under quadratic field map inhomogeneity

At first, we will consider the single-dimensional case. Let $f(u)$ be the magnetization of the object of interest. The MRI signal, in a perfect uniform B_0 field, ignoring T_1 and T_2 relaxations and after demodulation at the Larmor frequency ω_0 is

$$s(t) = \int f(u) e^{-i2\pi k(t)u} du$$

where, as customarily defined, $k(t) = \gamma/2\pi \int_0^t G(\xi)d\xi$ is the k -space trajectory.

Whenever there is an inhomogeneous field $B(u) = B_0 + p(u)$ as a function of space, the magnetization is modulated by a time-dependent phase. For the particular case of a quadratic inhomogeneity, $p(u) = p_2u^2 + p_1u + p_0$. In this case the signal equation becomes

$$s(t) = e^{-i2\pi p_0 t} \int f(u) e^{i\pi(-2p_2 t u^2 - 2(k(t) + p_1 t)u)} du \quad (3)$$

There is a remarkable similarity between this expression and the FrFT defined in (1). Consequently, it is natural to think that the FrFT can be used to reconstruct this data. Moreover, the FrFT is a theoretical tool that could allow us to extend the framework of MRI to quadratic fields, while recovering the homogeneous-field case as a particular case.

C. Link between the MRI Signal and the FrFT

In order to represent (3) in the form of (1), we define

$$\begin{aligned} \alpha(t) &= \cot^{-1}(-2p_2 t), \text{ and} \\ \rho(t) &= \frac{k(t) + p_1 t}{\csc \alpha(t)} = \frac{k(t) + p_1 t}{\sqrt{1 + 4p_2^2 t^2}} \end{aligned} \quad (4)$$

In this definition, both α and ρ are functions of time but we will often omit this for the sake of simplicity. We use $\alpha \in (0, \pi)$, which ensures $\csc \alpha > 0$, and \cot^{-1} is invertible. Therefore we can write these relations as $-2p_2 t = \cot \alpha$ and $-2(k(t) + p_1 t) = -2\rho \csc \alpha$. With these variables the signal in (3) becomes

$$s(t) = e^{-i2\pi p_0 t} \int f(u) e^{i\pi(u^2 \cot \alpha - 2\rho u \csc \alpha)} du$$

Using (1) we can express the signal equation as a time-varying order FrFT of the object

$$\begin{aligned} s(t) &= e^{-i2\pi p_0 t} C_\alpha(\rho)^{-1} f_a(\rho) \\ f_a(\rho) &= e^{i2\pi p_0 t} C_\alpha(\rho) s(t) \end{aligned} \quad (5)$$

Note that if α were constant and equal to $\pi/2$ (or $a = 1$), we recover the signal equation in terms of the standard Fourier transform.

The advantage of this relation is that we have a well known framework for working with quadratic terms in the magnetic field. In general, the inhomogeneity of the field will be better approximated by a second order polynomial. Additionally, second order terms naturally occur in coil design and are the most significant within second and upper orders.

D. The ρ - α space

The definition of α and ρ in (4) defines a parametric trajectory $(\rho(t), \alpha(t))$ in a space that we call ρ - α space. Since α is an angle, this space is conveniently represented in polar coordinates. The trajectory in ρ - α space starts

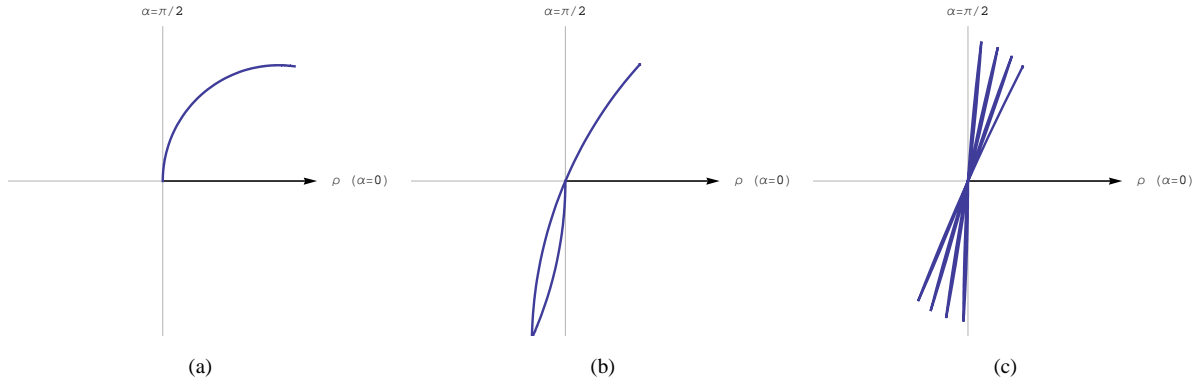


Fig. 1. Examples of typical trajectories over a quadratic field in the polar representation of ρ - α space. (a) A constant gradient can be represented as a circular path (b) A 2DFT bipolar gradient describes two circular arcs (c) The polar graph shows ρ - α space in the readout direction for seven readout echoes of an EPI trajectory.

immediately after the excitation ($t = 0$) in the frequency or Fourier direction ($\alpha = \pi/2$) and as time passes it curves toward the object axis ($\alpha = 0$).

In what follows we will analyze some common trajectories using this framework. For the sake of simplicity, we neglect the restrictions on the maximum slew rate.

1) *Constant gradient*: Let us assume that the readout gradient G_0 is constant and starts at $t = 0$, as would be the case in a projection reconstruction sequence. Assume also that the inhomogeneity is purely quadratic $p(u) = p_2 u^2$. Linear and constant terms can be ignored without loss of generality, because the first is equivalent to a change in the amplitude of the gradient and the second can be corrected during the signal demodulation. Then $k(t)$ would be $\int_0^t G_0 d\tau = G_0 t$ and the trajectory in ρ - α space would be

$$\begin{aligned}\alpha(t) &= \cot^{-1}(-2p_2 t) \\ \rho(t) &= \frac{k(t) + p_1 t}{\sqrt{1 + 4p_2^2 t^2}} = \frac{G_0 t}{\sqrt{1 + 4p_2^2 t^2}}\end{aligned}$$

which is the parametric form of a circumference centered at $(G_0/4p_2, 0)$. Fig. 1 (a) shows this trajectory starting in $t = 0$ at the origin. Assuming $p_2 < 0$, which resembles the typical case in which the intensity of the B_0 field is greater at the center of a magnet, we also observe that the trajectory asymptotically approaches the object axis ($\alpha = 0$) as t increases.

As expected, for small values of t , the trajectory deviates little from the frequency axis ($\alpha = \pi/2$), and therefore distortions due to field variations are small. This is consistent with the general knowledge that short readouts are less sensitive to inhomogeneities.

We also note that if p_2 tends to zero, the field inhomogeneity vanishes and the center of the circumference located

at $G_0/4p_2$ tends to infinity. Equivalently, the ρ - α trajectory becomes a straight line in the frequency direction

$$\begin{aligned}\alpha(t) &= \cot^{-1}(-2p_2t) = \frac{\pi}{2} \\ \rho(t) &= \frac{G_0t}{\sqrt{1+4p_2^2t^2}} = G_0t\end{aligned}$$

2) *Standard 2DFT readout*: Considering again that the field distortion is $p(u) = p_2u^2$, we now assume that the gradient is formed by a negative pulse of duration t_0 followed by a positive one, as is standard in 2DFT readouts.

In this case

$$k(t) = \int_0^t G(\tau)d\tau = \begin{cases} -G_0t & 0 < t < t_0 \\ G_0(t - 2t_0) & t_0 < t \end{cases}$$

Consequently, the trajectory in ρ - α space is given by

$$\begin{aligned}\alpha(t) &= \cot^{-1}(-2p_2t) \\ \rho(t) &= \frac{1}{\sqrt{1+4p_2^2t^2}} \times \begin{cases} -G_0t & 0 < t < t_0 \\ G_0(t - 2t_0) & t_0 < t \end{cases}\end{aligned}$$

This trajectory is formed by two circular arcs. The trajectory describes one arc for the negative gradient centered at $(-G_0/4p_2, 0)$ and continues to the other one centered at $(G_0/4p_2, -G_0t_0)$, which corresponds to the positive gradient, as shown in Fig. 1 (b).

3) *EPI readout*: If the gradient were a train of negative and positive pulses as is used in Echo Planar Imaging

$$G(t) = \begin{cases} -G_0 & \text{for } 0 < t < t_0, 3t_0 < t < 5t_0, \dots \\ G_0 & \text{for } t_0 < t < 3t_0, 5t_0 < t < 7t_0, \dots \end{cases}$$

the described ρ - α trajectory would be composed by a series of circular arcs centered at $(\pm G_0/4p_2, \mp jG_0t_0/2)$, $j = 0, 1, 2, \dots$ as shown in Fig. 1 (c).

4) *Spectroscopy*: If the sequence has no gradients, as in a pure spectroscopic acquisition, the trajectory will only depend on the linear term of the field deviation p_1

$$\begin{aligned}\alpha(t) &= \cot^{-1}(-2p_2t) \\ \rho(t) &= \frac{k(t) + p_1t}{\sqrt{1+4p_2^2t^2}} = \frac{p_1t}{\sqrt{1+4p_2^2t^2}}\end{aligned}$$

and will have the shape shown in Fig. 1 (a), centered at $(p_1/4p_2, 0)$. If $p_1 = 0$, the trajectory is a singularity at the origin of the ρ - α space. In this case it is more convenient to represent the space in Cartesian coordinates (ρ, a) , and the readout trajectory $\rho = 0$ becomes equivalent to acquire the continuous component of the FrFT for the orders a .

III. EXTENSION TO TWO DIMENSIONS

To extend the correspondence of the signal equation to the FrFT definition we employ the fact that the latter is separable and easily written in vector form. In two dimensions the FrFT is [14]

$$f_{\mathbf{a}}(\boldsymbol{\rho}) = C_{\boldsymbol{\alpha}}(\boldsymbol{\rho}) \int f(\mathbf{u}) e^{i\pi(\mathbf{u}^T \mathbf{A} \mathbf{u} - 2\mathbf{u}^T \mathbf{B} \boldsymbol{\rho})} d\mathbf{u}$$

with

$$\mathbf{u} = \begin{bmatrix} u \\ v \end{bmatrix}, \quad \boldsymbol{\rho} = \begin{bmatrix} \rho_u \\ \rho_v \end{bmatrix}, \quad \mathbf{a} = \begin{bmatrix} a_u \\ a_v \end{bmatrix}, \quad \boldsymbol{\alpha} = \mathbf{a} \frac{\pi}{2} = \begin{bmatrix} \alpha_u \\ \alpha_v \end{bmatrix}$$

$$\mathbf{A} = \begin{bmatrix} \cot \alpha_u & 0 \\ 0 & \cot \alpha_v \end{bmatrix}, \quad \mathbf{B} = \begin{bmatrix} \csc \alpha_u & 0 \\ 0 & \csc \alpha_v \end{bmatrix}$$

and $C_{\boldsymbol{\alpha}}(\boldsymbol{\rho}) = \sqrt{1 - i \cot \alpha_u} \sqrt{1 - i \cot \alpha_v} e^{i\pi \boldsymbol{\rho}^T \mathbf{A} \boldsymbol{\rho}}$.

To write the signal equation in 2D we write the field distortion as $p(\mathbf{u}) = \mathbf{u}^T \mathbf{p}_2 \mathbf{u} + \mathbf{u}^T \mathbf{p}_1 + p_0$, with

$$\mathbf{p}_1 = \begin{bmatrix} p_{1u} \\ p_{1v} \end{bmatrix} \quad \text{and} \quad \mathbf{p}_2 = \begin{bmatrix} p_{2u} & 0 \\ 0 & p_{2v} \end{bmatrix}$$

so that it becomes

$$s(t) = e^{-i2\pi p_0 t} \int f(\mathbf{u}) e^{i\pi(-2\mathbf{u}^T \mathbf{p}_2 \mathbf{u} - 2\mathbf{u}^T (\mathbf{k}(t) + \mathbf{p}_1 t))} d\mathbf{u} \quad (6)$$

with $\mathbf{k}(t) = [k_u(t) \ k_v(t)]^T$. Note that we also assumed that the field distortion is diagonal in the coordinate axis, i.e. the terms outside the diagonal of \mathbf{p}_2 are zero in order to match the separable form of the FrFT.

Remark that both \mathbf{A} and \mathbf{B} are diagonal matrices that depend on $\boldsymbol{\alpha}$. We can proceed as we did previously to define the four-dimensional ρ - α space using the change of variables:

$$\begin{aligned} \cot \alpha_u &= -2p_{2u} t \\ \cot \alpha_v &= -2p_{2v} t \\ \rho_u \csc \alpha_u &= k_u(t) + p_{1u} t \\ \rho_v \csc \alpha_v &= k_v(t) + p_{1v} t \end{aligned}$$

which is equivalent to solve for $\boldsymbol{\alpha}$ and $\boldsymbol{\rho}$ the matrix equations $\mathbf{A}(\boldsymbol{\alpha}) = -2\mathbf{p}_2 t$ and $\mathbf{B}(\boldsymbol{\alpha})\boldsymbol{\rho} = \mathbf{k}(t) + \mathbf{p}_1 t$. Finally, the signal equation can be expressed in terms of a 2D varying-order FrFT as

$$s(t) = e^{-i2\pi p_0 t} C_{\boldsymbol{\alpha}}(\boldsymbol{\rho})^{-1} f_{\mathbf{a}}(\boldsymbol{\rho})$$

IV. RECONSTRUCTION

In the FrFT framework, the reconstruction problem requires to know both the pseudo-frequency and the transform order where the data was acquired. These can be determined using (4). The object will be the solution to the inverse of (5) (ignoring the constant field deviation p_0)

$$\begin{aligned} \hat{f}(u) &= \mathcal{F}^{-a} \{ f_{a(t)}(\rho(t)) \} (u) \\ &= \mathcal{F}^{-a} \{ C_{\alpha(t)}(\rho(t)) s(t) \} (u) \end{aligned}$$

In this expression we have made explicit the time dependence of α . This dependency implies that the fractional order changes with time and therefore a inverse FrFT is not feasible. We analyze three different reconstruction approaches: standard inverse Fourier reconstruction; inverse fractional Fourier reconstruction; and variable order

inverse fractional Fourier reconstruction. The difference between these reconstructions is the assumption they make on where the data is placed in the ρ - α space. In Fig. 2 we show the actual ρ - α space trajectory and the assumption of the reconstruction scheme for a standard 2DFT readout.

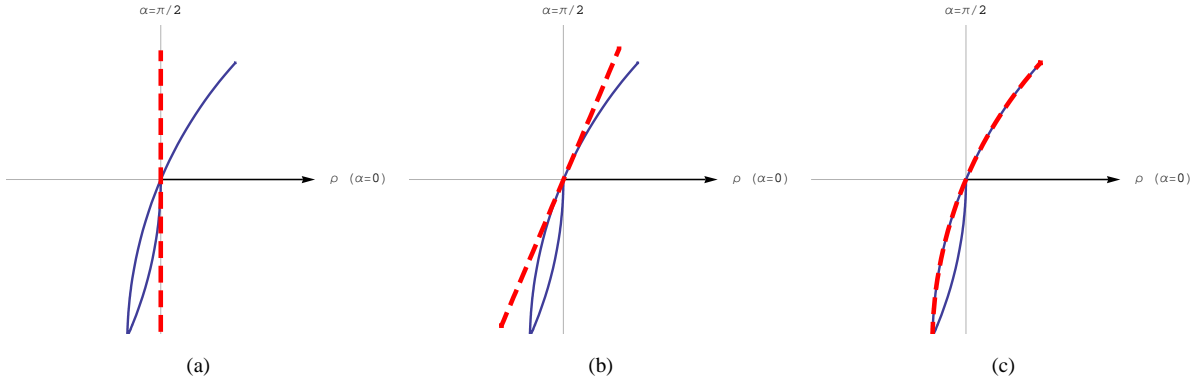


Fig. 2. Example of a one dimensional 2DFT trajectory in the polar representation of ρ - α space represented by the continuous line and its reconstruction interpretation represented by the dashed line. (a) Standard Fourier interpretation (b) Fractional Fourier interpretation (c) Variable order inverse fractional Fourier interpretation.

A. Standard Inverse Fourier Reconstruction

The first approach is to perform the reconstruction by using the standard inverse Fourier transform. This is equivalent to assume that $\alpha \equiv \pi/2$, $\cot \alpha \equiv 0$ and $C_{\pi/2}(\rho) \equiv 1$. The reconstructed object is

$$\hat{f}_1(u) = \mathcal{F}^{-1} \{s(t)\} (u)$$

The samples are acquired in the curved trajectory but are interpreted as being in the frequency axis (vertical dashed line of Fig. 2(a)). The distortions in the image will depend on how much the reconstruction locations differ from the sampling locations.

B. Inverse Fractional Fourier Reconstruction

The second approach is to assume that the samples are being acquired at a constant order, which can be thought as a tangent approximation in the ρ - α plane. This approach has two advantages: (i) the reconstruction and sampling locations are closer; and (ii) the inverse expression is exactly an inverse FrFT

$$\hat{f}_{\bar{a}}(u) = \mathcal{F}^{-\bar{a}} \{C_{\bar{\alpha}}(\rho(t)) s(t)\} (u)$$

where \bar{a} (or $\bar{\alpha}$) is the order (or angle for the tangent line) at the origin. As we will show in Section VI, this reconstruction provides a better approximation to the real object since it improves the accuracy of the reconstructed phase over the standard Fourier reconstruction. However, the magnitude is the same as the one obtained with the standard Fourier reconstruction. Using the definitions in (1) and (2) it can be seen that

$$\hat{f}_{\bar{a}}(u) = e^{-i\pi u^2 \cot \bar{\alpha}} |\csc \bar{\alpha}| \int s(t) e^{i2\pi u \rho \csc \bar{\alpha}} d\rho \quad (7)$$

C. Variable Order Inverse Fractional Fourier Reconstruction

Finally, the third approach is to use the actual locations where the data was acquired. To solve the variable order inverse problem we propose a discrete approach, which fits well with the discrete samples and can also provide a continuous reconstruction. Each sample in ρ - α space (ρ_n, α_n) acquired at $t = t_n$ corresponds to one coefficient of the FrFT of order $a_n = 2\alpha_n/\pi$. These coefficients can be thought as the expansion of the object on the bases formed by the ‘‘chirp’’ functions. These functions are given by the inverse FrFT of order a_n of a delta function located at $\rho = \rho_n$ [14]:

$$\begin{aligned}\Delta_{-a_n}(u) &= \mathcal{F}^{-a_n} \{\delta(\rho - \rho_n)\}(u) \\ &= C_{\alpha_n}^*(\rho_n) e^{-i\pi(u^2 \cot \alpha_n - 2u\rho_n \csc \alpha_n)}\end{aligned}$$

where $*$ denotes complex conjugate. Recalling that the samples (ignoring again the constant field shift, p_0) are defined by

$$f_{a_n}(\rho_n) = C_{\alpha_n}(\rho_n)s(t_n)$$

we have an estimation of the object as the weighted sum of all contributions.

$$\begin{aligned}\hat{f}_\alpha(u) &= \sum_{n=1}^N f_{a_n}(\rho_n)\Delta_{-a_n}(u) \\ &= \sum_{n=1}^N |\csc \alpha_n| s(t_n) e^{-i\pi(u^2 \cot \alpha_n - 2u\rho_n \csc \alpha_n)}\end{aligned}$$

We assume a uniform sampling density, otherwise it would be necessary to incorporate a factor proportional to $\dot{\rho}(t_n)$ which arises from the underlying discretization of the inverse FrFT integral by Riemann sums.

The object $\hat{f}_\alpha(u)$ can be evaluated for any continuous value of u . Note that if we substitute α_n by $\pi/2$ this formula becomes the definition of the Discrete Frequency Fourier Transform (DFFT), or the Discrete Fourier Transform (DFT), if u is also evaluated at discrete values. If α_n is substituted by another fixed angle, other than $\pi/2$, the reconstruction is also the DFFT, but with an extra phase and an additional constant scaling factor. This is the discrete version of the inverse Fractional Fourier Transform.

The 2D extension of this reconstructions is:

$$\hat{f}(\mathbf{u}) = \sum_{n=1}^N |\det(\mathbf{B}_n)| s(t_n) e^{-i\pi(\mathbf{u}^T \mathbf{A}_n \mathbf{u} - 2\mathbf{u}^T \mathbf{B}_n \rho_n)} \quad (8)$$

D. Units

So far we have used ρ and u as dimensionless variables. To ensure the validity of the former analysis and extend it to practical cases, we use the normalization $u = x/q$ in which

$$f(u) = f(x/q) = \sqrt{q}\tilde{f}(x) \quad (9)$$

with $\tilde{f}(x)$ the dimensional object. The scale parameter q has the same dimension as x . In the discrete case, we need longitudes in ρ to be independent of α , which can be achieved by setting $q = FOV/\sqrt{N}$ [25] where FOV

is the field of view in distance units and N is the number of samples. This normalization is independently applied for each dimension.

V. EXPERIMENTS AND METHODS

All MRI images mentioned in this section were acquired in a Philips Intera 1.5T scanner. Linear shimming was disabled during all acquisitions and no higher order active shimming was used. The sequences were performed without any consideration about ρ - α space, using mostly default parameters from pre-loaded sequences in the system. Complex-valued image reconstructions were performed off-line.

A. Analytical phantom

In our first experiment, the MR signal for a two dimensional (2D) analytical magnetization phantom was simulated by numerically evaluating (6) using adaptive quadrature in MATLAB [26], nesting a one-dimensional evaluation for each dimension. The phantom was designed as a simplified version of a real reference phantom with the same dimensions. The acquisition time of each sample and k -space locations were determined considering 2DFT gradients used in standard Fourier acquisition. We simulated a cartesian matrix of 256×256 samples with a field of view (FOV) of 25.6×25.6 cm and echo time $TE = 56$ ms. Each complete readout in the sequence takes 28 ms.

Two signals were simulated, the first with a uniform B_0 field and the second with a quadratic field. The quadratic deviation was chosen to emulate the quadratic component for a real phantom, but doubling its values to increase the effect of the distortion in the simulation, and at the same time keeping it within a valid physical range.

B. MRI phantom

In another experiment, we scanned an MRI phantom using a fast field echo (FFE) echo-planar imaging (EPI) sequence, with a scan matrix of 128×128 samples, image FOV of 24×24 cm, slice thickness 5 mm, flip angle 23° , repetition time $TR = 650$ ms and echo time $TE = 41$ ms. This data was acquired with a number of sample averages (NSA) of 16 using a Q-body coil. The EPI factor in this sequence is 63. Each complete readout in this sequence took 76 ms.

C. In-vivo study

An *in-vivo* study was done scanning the brain of a volunteer, the images were acquired using the same sequence used for the phantom study, except from NSA which was now 8 and from the receiving coil which was now a standard quadrature head coil. A slightly angled transversal slice of the brain was selected.

D. Field maps

In each experiment, structural images were acquired with short readout time sequences to minimize the effect of field inhomogeneity. The magnetic field was measured in each location from phase differences in two images

with different echo time, using $\Delta\omega(x, y) = \Delta\phi(x, y)/\Delta\text{TE}$ [27] with a short ΔTE to avoid phase wrapping in the resulting field map.

To fit quadratic functions to the field maps, we used a maximum likelihood method that minimizes the weighted squared error between the measured field map and a parametric separable second order polynomial evaluated at corresponding positions. The weights were the mean of the corresponding pixels in the magnitude of the images from which the phase difference had been obtained. This ensures that the field map information was incorporated correctly depending on the local intensity of the signal and its signal to noise ratio. In the case of the *in-vivo* study, a region of interest was defined by setting to zero the weighting outside it.

In the phantom study, the field map was determined along a structural reference image using $\Delta\text{TE} = 3$ ms and TR and TE equal to 14 and 6.1 ms respectively. A transversal slice of the physical phantom was selected for this study.

For the *in-vivo* study, the structural reference image was obtained with TR and TE equal to 17 and 6.2 ms respectively for the same field of view and resolution. The field map was computed with $\Delta\text{TE} = 6$ ms. The anatomy causes further field deviations which cannot be approximated by the fitted function for the entire FOV. We therefore used an elliptical region of interest (ROI) where the field is mainly quadratic and the approximation is suitable to demonstrate the proposed reconstruction.

Field maps and profiles displayed in all figures in Section VI share the same color scaling, mapping the entire range to a 180 Hz difference, with the lowest and highest intensities mapped to -140 Hz and 40 Hz respectively. To display the measured field maps and phase images, the field map value was set to zero wherever the intensity of the signal was below 5% of its maximum value.

E. Image reconstruction

In all experiments, image reconstruction was performed by estimating the magnetization of the object computing (8) and evaluating \mathbf{u} at the corresponding positions in dimensionless coordinates. Distance units of the results were scaled using (9) to map the estimated object into the dimensional coordinates. Three different reconstruction schemes were used in each experiment, producing three object estimations according to diagrams (a), (b) and (c) in Fig. 2. The first one is standard inverse Fourier (FT) reconstruction and used $\alpha_{un} = \alpha_{vn} = \pi/2, \forall n = 1 \dots N$. The second one, inverse fractional Fourier (FrFT) reconstruction, used $\alpha_{un} = \bar{\alpha}_u, \alpha_{vn} = \bar{\alpha}_v, \forall n = 1 \dots N$ with $\bar{\alpha}_u$ and $\bar{\alpha}_v$ equal to the angles at the origin of the four-dimensional ρ - α space during the readout. Variable order inverse fractional Fourier (VO-FrFT) reconstruction took into account the exact position in ρ - α space of each sample.

VI. RESULTS

A. Analytical phantom

One can observe the distortions produced by a quadratic field when using the standard Fourier reconstruction, by comparing Figures 3 (a) and (b). We appreciate a geometric distortion, characteristic of data acquired under

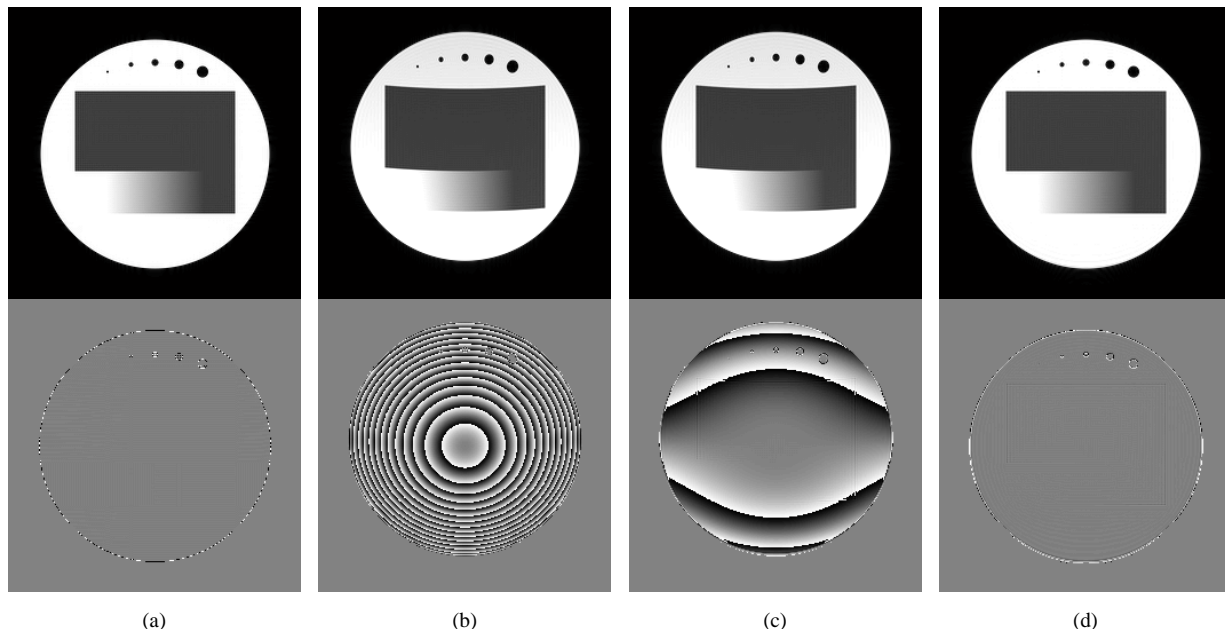


Fig. 3. Reconstruction results for 2DFT simulations with an isotropic quadratic field. Each column shows magnitude and phase images with the same color scaling. Magnitude moves from 0 to 1 and the from $-\pi$ to π . Phase values have been set to zero when magnitude is below 5% of maximum. (a) Ideal reconstruction for a homogeneous field simulation and standard inverse Fourier reconstruction. The remaining columns show reconstructions for a quadratic field simulation. (b) Standard inverse Fourier reconstruction. (c) Inverse fractional Fourier reconstruction with constant α approximation for each echo. (d) Variable order inverse fractional Fourier reconstruction considering exact trajectory.

field inhomogeneity, which is proportional to the local field deviation from the central frequency. The phase of the reconstructed image has a complex quadratic modulation but the analytical phantom did not have phase. An intensity nonuniformity distortion is also noted, in which the distorted image has an intensity approximately 12% lower in the upper section of the object and a similar inverse variation in the lower section.

The three reconstructions are shown in Fig. 3 (b), (c) and (d). As expected by means of (7), the reconstruction result for inverse fractional Fourier (FrFT) reconstruction in (c) shows identical magnitude than the standard inverse Fourier (FT) reconstruction (b) but with a phase much closer to the actual phase. In (d), variable order inverse fractional Fourier (VO-FrFT) reconstruction shows correction of image distortions in magnitude and phase, including the geometric distortion.

B. MRI phantom

In the MRI phantom study, we have found that the particular combination of our MR system with its intrinsic inhomogeneity and the scanned phantom produced a field map that resembles an isotropic quadratic function with its highest intensity in the center of the magnet as shown in Fig. 4.

In this study, the phase information of the object is unknown since we cannot acquire it with the same contrast as the distorted object but without the effect of the quadratic field map. We will compare the magnitude of the reconstructions of the distorted signal with the magnitude of a low distortion image acquired with short readouts.

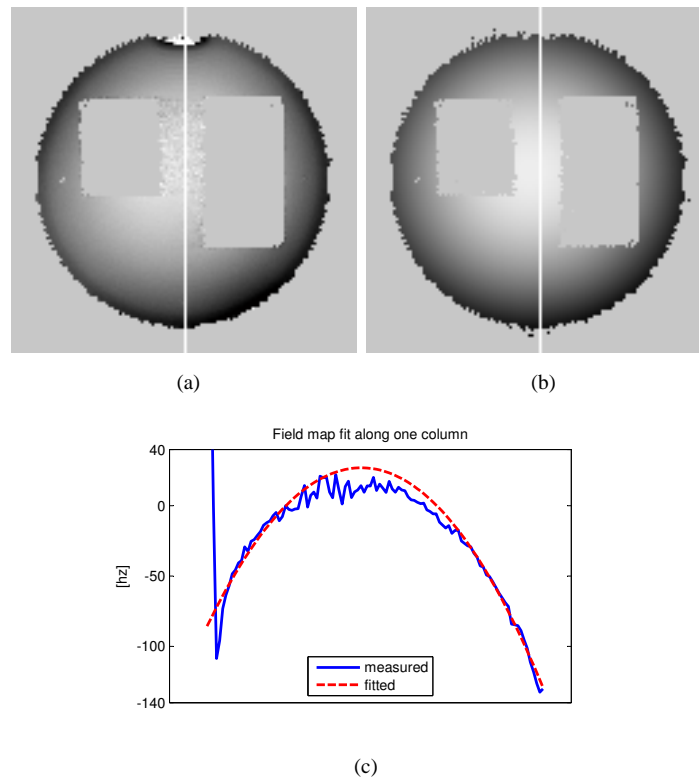


Fig. 4. Field map fit for MRI Phantom. (a) Measured field map. (b) Fitted field map. (c) Along the marked column, the measured magnetic field (solid line) can be approximated by a quadratic function (dashed line).

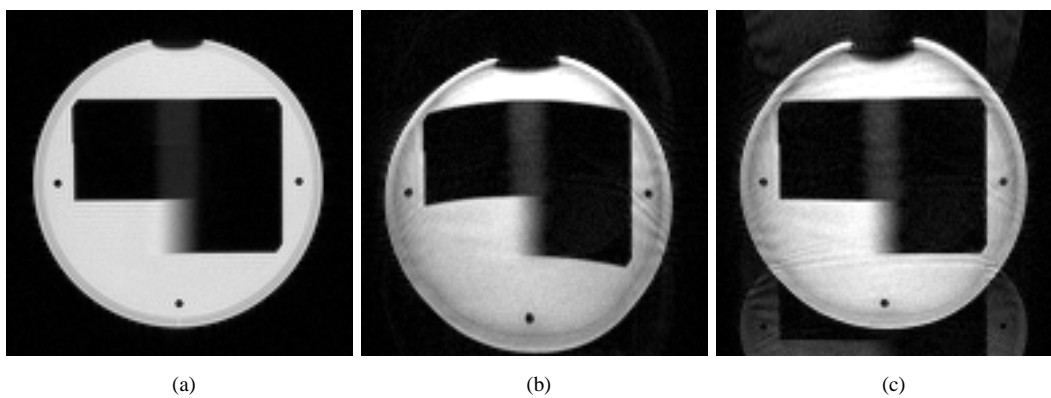


Fig. 5. Reconstruction results for MRI Phantom under quadratic field. Geometric distortions shown in (b) obtained using a standard Fourier reconstruction can be corrected in (c) using variable order fractional Fourier reconstruction, compared to a low distortion image (a).

The FT reconstruction shown in Fig. 5 (b) produces geometric and intensity distortions similar to those observed in the simulation study for a quadratic field (Fig. 3 (b)). Figure 5 also shows that the VO–FrFT reconstruction (c), partially corrects these distortions, improving the geometry and intensity of the estimation when comparing both reconstructions against the low distortion image (a). Ghosting artifacts are visible in (c) which we do not fully understand, but believe to be related to an incomplete phase correction typically used to reduce the EPI ghosting artifact.

As expected, magnitudes of the fractional Fourier reconstruction and standard Fourier reconstruction are identical, therefore the first was omitted from the figures.

C. In–vivo study

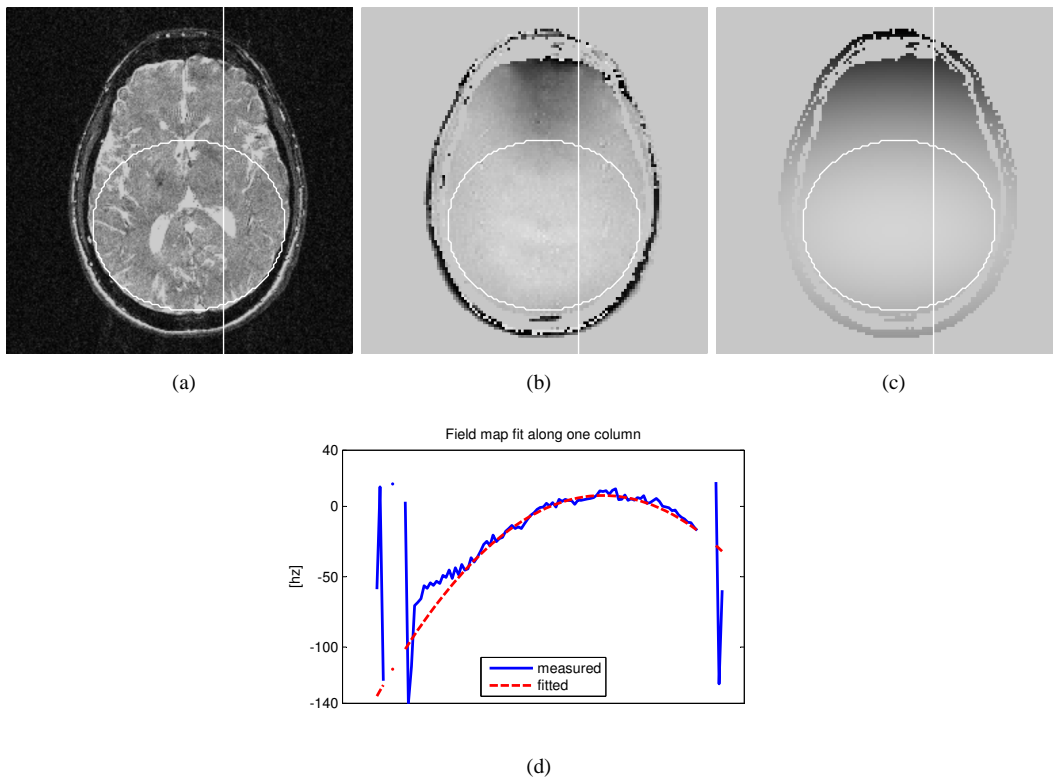


Fig. 6. Field map fit for *in-vivo* study. (b) Measured field map. (c) Fitted field map. Within the elliptical ROI in (a), the measured magnetic field can be approximated by a quadratic function as shown in (d) with solid and dashed lines respectively for the marked column.

With the volunteer experiment we found the magnetic field to vary smoothly inside the brain. In particular, the field can be approximated by a quadratic function within an elliptical region of interest (ROI) as shown in Fig. 6. The VO–FrFT reconstruction partially corrects most of the geometric distortions present in the FT reconstruction as can be seen in Fig. 7, especially in the regions in which the fitted quadratic function is a close approximation of the field map. To facilitate the comparison we have superimposed on all reconstructions in Fig. 7 contours that show the actual location of key features taken from a reference image (a).

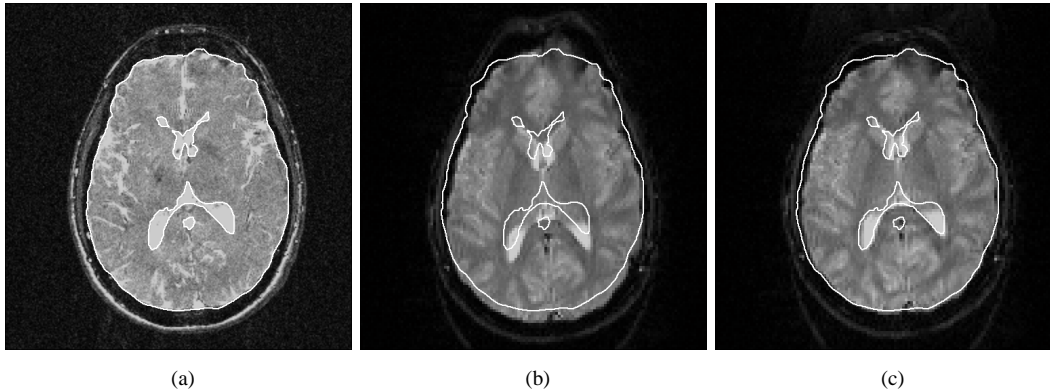


Fig. 7. Reconstruction results for *in-vivo* study. The superimposed contour shows location of some key features in the reference image (a). (b) Standard Fourier reconstruction. (c) Variable order Fourier reconstruction with corrected quadratic field inhomogeneity.

VII. CONCLUSIONS

Traditionally, MRI reconstruction is performed applying an inverse Fourier Transform (FT) of the acquired MR signal. This method rests on the base that the object has been magnetized with a perfectly uniform magnetic field. In practice, it is not possible to get a uniform field because of physical restrictions and susceptibility variations at the scanned object. This is a critical problem as the MR community is pushing for getting short-bore and high-field MR systems, which are exactly the kind of factors that tend to increase field inhomogeneities. Additionally, sequences with long acquisition windows, such as EPI and spiral, are increasingly used. These sequences are severely affected by inhomogeneity-related artifacts. Modern MR systems always include linear field corrections and higher-order polynomial field corrections are getting a common feature. It is therefore reasonable to think that main magnetic fields are not intrinsically uniform. In fact, in all our experiments our magnet showed a nearly quadratic behavior.

We present a new, strongly supported framework for quadratic inhomogeneity MR signal analysis based on the Fractional Fourier Transform (FrFT). It restores the theoretical relation between image space and quadratic magnetic field signal space, allowing native second order field image reconstruction (or correction). This transform, which is a generalization of the FT, has a quadratic term in its integral kernel, so that there is a natural link between the signal obtained from an object magnetized with a quadratic field and its FrFT.

This new framework and the ρ - α space we introduce give a visual insight to the MR acquisition process and also, provide a meaningful graphical representation that shows the relation between the image domain, the standard k -space and FrFT domains.

Our experiments showed that our proposed method, the variable order fractional Fourier reconstruction (VO-FrFT), can effectively reconstruct MRI signals under nearly quadratic magnetic fields, without being affected by the geometric distortions that appear when those signals are reconstructed by the standard FT scheme.

One effect of analyzing MR data using ρ - α space is that k is scaled down by a factor $\csc \alpha \geq 1$. This scaling is not homogeneous in k -space but depends on the time map of the sequence. For a given sequence planned for

ordinary k -space acquisition, this fact traduces into a resolution loss. These resolution losses can be eliminated using stronger gradients with an ordinary sequence or modifying the sequence to fill ρ - α space accounting for the effect of the time map in resolution.

Trajectories should be modified to fill ρ - α space in an optimal way for resolution of the image. Theoretical advances are also needed to replace the Nyquist sampling rate condition from k -space with a similar condition which would indicate how information density is distributed along ρ - α space.

Our approach based on the Fractional Fourier Transform gives a new theoretical MR framework between image space and signal space for quadratic field MR systems, allowing native image reconstruction for second order main fields. Hopefully, this new approach will reduce the hardware complexity of MR systems, since the second order terms in the main magnetic field would no longer be a concern.

ACKNOWLEDGMENT

The authors would like to thank CONICYT for their funding through the grants FONDECYT 1070674, FONDEF D05I10358 and PROYECTO ANILLO PBCT-ACT-13.

REFERENCES

- [1] Z. Liang and P. C. Lauterbur, *Principles of magnetic resonance imaging: a signal processing perspective*. Bellingham, Washington: SPIE Optical Engineering Press, 2000.
- [2] H. Kalinowski, S. Berger, and S. Braun, *Carbon-13 NMR spectroscopy*. Chichester: Wiley, 1988.
- [3] P. Veldine, "The whole body 11.7 t mri magnet for iseu/inumac project," *IEEE Transactions on Applied Superconductivity*, vol. 18, no. 2, p. 868, 2008.
- [4] T. Vaughan, L. DelaBarre, C. Snyder, J. Tian, C. Akgun, D. Shrivastava, W. Liu, C. Olson, G. Adriany, J. Strupp, P. Andersen, A. Gopinath, P. F. van de Moortele, M. Garwood, and K. Ugurbil, "9.4t human mri: preliminary results," *Magnetic Resonance in Medicine*, vol. 56, no. 6, pp. 1274–1282, Dec 2006.
- [5] J. A. Akel, M. Rosenblitt, and P. Irarrazaval, "Off-resonance correction using an estimated linear time map," *Magnetic resonance imaging*, vol. 20, no. 2, pp. 189–198, Feb 2002.
- [6] W. Chen and C. H. Meyer, "Semiautomatic off-resonance correction in spiral imaging," *Magnetic Resonance in Medicine*, vol. 59, no. 5, pp. 1212–1219, May 2008.
- [7] W. Chen, C. T. Sica, and C. H. Meyer, "Fast conjugate phase image reconstruction based on a chebyshev approximation to correct for b0 field inhomogeneity and concomitant gradients," *Magnetic Resonance in Medicine*, vol. 60, no. 5, pp. 1104–1111, Nov 2008.
- [8] J. A. Fessler, S. Lee, V. T. Olafsson, H. R. Shi, and D. C. Noll, "Toeplitz-based iterative image reconstruction for mri with correction for magnetic field inhomogeneity," *IEEE Transactions on Signal Processing*, vol. 53, no. 9, pp. 3393–3402, 2005.
- [9] P. Irarrazabal, C. H. Meyer, D. G. Nishimura, and A. Macovski, "Inhomogeneity correction using an estimated linear field map," *Magnetic Resonance in Medicine*, vol. 35, no. 2, pp. 278–282, Feb 1996.
- [10] J. V. Manjón, J. J. Lull, J. Carbonell-Caballero, G. García-Martí, L. Martí-Bonmatí, and M. Robles, "A nonparametric mri inhomogeneity correction method," *Medical image analysis*, vol. 11, no. 4, pp. 336–345, 8 2007.
- [11] D. C. Noll, J. A. Fessler, and B. P. Sutton, "Conjugate phase mri reconstruction with spatially variant sample density correction," *IEEE Transactions on Medical Imaging*, vol. 24, no. 3, pp. 325–336, 2005.
- [12] B. P. Sutton, D. C. Noll, and J. A. Fessler, "Fast, iterative image reconstruction for mri in the presence of field inhomogeneities," *IEEE Transactions on Medical Imaging*, vol. 22, no. 2, pp. 178–188, 2003.
- [13] U. Vovk, F. Pernus, and B. Likar, "Mri intensity inhomogeneity correction by combining intensity and spatial information," *Physics in Medicine and Biology*, vol. 49, no. 17, pp. 4119–4133, Sep 7 2004.

- [14] H. M. Ozaktas, M. A. Kutay, and Z. Zalevsky, *The fractional Fourier transform with applications in optics and signal processing*. Chichester; New York: Chichester, New York: Wiley, 2001.
- [15] H. M. Ozaktas and D. Mendlovic, "Fourier transforms of fractional order and their optical interpretation," *Optics Communications*, vol. 101, no. 3-4, pp. 163–169, 1993.
- [16] —, "Fractional fourier optics," *Journal of the Optical Society of America A*, vol. 12, no. 4, p. 743, 1995.
- [17] I. S. Yetik, "Image representation and compression with the fractional fourier transform," *Optics Communications*, vol. 197, no. 4-6, p. 275, 2001.
- [18] C. Candan, M. A. Kutay, and H. M. Ozaktas, "The discrete fractional fourier transform," *IEEE Transactions on Signal Processing*, vol. 48, no. 5, p. 1329, 2000.
- [19] H. M. Ozaktas and U. Sumbul, "Interpolating between periodicity and discreteness through the fractional fourier transform," *IEEE Transactions on Signal Processing*, vol. 54, no. 11, pp. 4233–4243, 2006.
- [20] A. Bultheel, "Computation of the fractional fourier transform," *Applied and Computational Harmonic Analysis*, vol. 16, no. 3, p. 182, 2004.
- [21] H. E. Guven, H. M. Ozaktas, A. E. Cetin, and B. Barshan, "Signal recovery from partial fractional fourier domain information and its applications," *IET Signal Processing*, vol. 2, no. 1, p. 15, 2008.
- [22] H. M. Ozaktas, B. Barshan, D. Mendlovic, and L. Onural, "Convolution, filtering, and multiplexing in fractional fourier domains and their relation to chirp and wavelet transforms," *Journal of the Optical Society of America A*, vol. 11, no. 2, p. 547, 1994.
- [23] H. M. Ozaktas, O. Arikan, M. A. Kutay, and G. Bozdagt, "Digital computation of the fractional fourier transform," *IEEE Transactions on Signal Processing*, vol. 44, no. 9, p. 2141, 1996.
- [24] H. M. Ozaktas, B. Barshan, and D. Mendlovic, "Convolution and filtering in fractional fourier domains," 1994.
- [25] A. Koc, H. M. Ozaktas, C. Candan, and M. A. Kutay, "Digital computation of linear canonical transforms," *IEEE Transactions on Signal Processing*, vol. 56, no. 6, pp. 2383–2394, 2008.
- [26] L. F. Shampine, "Vectorized adaptive quadrature in matlab," *Journal of Computational and Applied Mathematics*, vol. 211, no. 2, pp. 131–140, 2008.
- [27] E. Schneider and G. Glover, "Rapid in vivo proton shimming," *Magnetic Resonance in Medicine*, vol. 18, no. 2, pp. 335–347, Apr 1991.